

Characteristics and NO_x formation mechanism of thermodiffusively unstable premixed hydrogen flames

By X. Wen[†], L. Berger[†], K. Maeda, J. Wang, A. Parente[‡] AND H. Pitsch[†]

In this study, the formation of NO_x pollutants in thermodiffusively unstable premixed hydrogen flames is investigated. At first, the overall NO_x formation characteristics are analyzed, and the effects of the computational setup (2D vs. 3D) on the NO_x formation are quantified. Then, reaction path analyses are conducted to identify the relevant reaction pathways that make important contributions to the formation of NO_x pollutants. Finally, the performance of the flamelet model in predicting the NO_x species is evaluated through an *a-priori* analysis. The results show that the computational setup has significant effects on NO_x formation, e.g., the peak value difference of NO mass fraction is around 50%. For the condition studied, the NNH and N_2O pathways are dominant for the NO formation. The flamelet model gives accurate predictions of NO_x species in the positively curved region, while discrepancies exist in the negatively curved region.

1. Introduction

Hydrogen is drawing rapidly growing attention around the world. The advantage of the deployment of hydrogen is that its thermochemical conversion does not lead to emissions of the greenhouse gas CO_2 . However, nitrogen oxides (NO_x) can be formed during the combustion of hydrogen in air. For non-premixed or fuel-rich premixed combustion, the formation of NO_x by the thermal pathway is found to be the primary reaction pathway due to the high temperatures (Correa 1993). In fuel-lean premixed hydrogen flames, NO_x emissions can be reduced due to the overall lower flame temperatures.

For fuel-lean hydrogen combustion, the thermodiffusive instability, which is associated with the disparity between the heat flux leaving the reaction zone and the mass flux of the fuel entering the reaction zone, is significant due to the lower effective Lewis number of the unburned mixture (Law & Sung 2000; Matalon 2007). The intrinsic instability in premixed hydrogen flames leads to cellular structures, which directly influence local heat release, local fuel air ratio and, hence, the distributions of temperature in the burned gas region. The NO_x formation reactions take place within the flame, and their significance depends on the local temperatures. NO_x pollutants are expected to be enhanced in super-adiabatic regions and suppressed in extinguished pockets, which leads to a complicated global NO_x formation mechanism. However, the underlying physics governing the interactions between the thermodiffusive instability and NO_x formation are still unclear.

For thermodiffusively unstable premixed hydrogen flame, various direct numerical simulations (DNSs) have been conducted; see, for example, Matalon (2007), Day *et al.* (2011b), Berger *et al.* (2019, 2022), and Wen *et al.* (2022a,b). However, most of these

[†] Institute for Combustion Technology, RWTH Aachen University, Germany

[‡] Brussels Institute for Thermal-Fluid Systems and Clean Energy, Université Libre de Bruxelles, Belgium

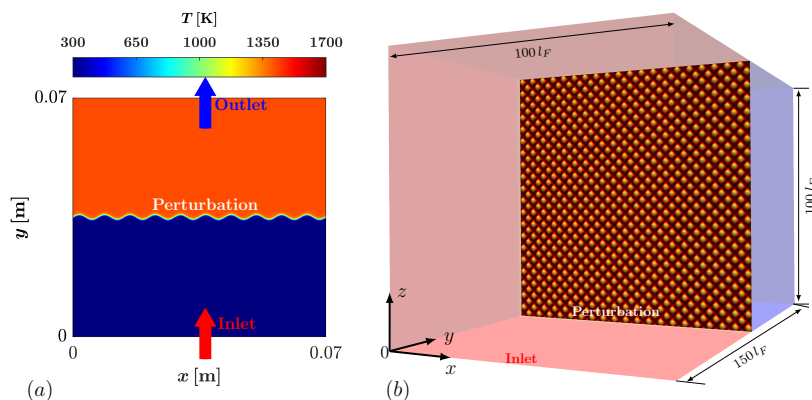


FIGURE 1. Numerical setups of the planar thermodiffusively unstable premixed hydrogen flames in the (a) 2D and (b) 3D computational domains. The isosurface of $T_{iso} = 1000$ K colored by the local value of Y_{NO} is shown in (b) for illustration of the perturbed initialization fields, with H_2 mass fraction being superimposed as the background color.

studies adopted 2D configurations to approximate the combustion behavior, or NO_x formation was not considered. As the effects of strain rate and curvature are significantly different in three dimensions, it is desirable to investigate the NO_x formation mechanism of thermodiffusively unstable premixed hydrogen flames in a 3D computational domain. For this, the 3D simulation domain of Berger *et al.* (2022) is significantly enlarged to capture the full range of possible flame corrugations.

Modeling a thermodiffusively unstable premixed hydrogen flame is challenging due to the wide ranges of scales, strain rate and curvature (Wen *et al.* 2022*a,b*). Modeling NO_x formation is even more difficult due to the existence of different reaction pathways, i.e., thermal-NO, NNH and N_2O pathways (Glarborg *et al.* 2018). The interactions between the flame-intrinsic instabilities and the various NO_x formation pathways challenge combustion models. The performance of the flamelet model (Peters 1984) in predicting NO_x formation in a thermodiffusively unstable premixed hydrogen flame was rarely evaluated in previous studies.

The motivation of the present work is to investigate the NO_x formation in the thermodiffusively unstable premixed hydrogen flame through DNS for both 2D and 3D computational domains to understand the effect of dimensionality. Based on the DNS data sets, the characteristics of NO_x formation in the thermodiffusively unstable premixed hydrogen flame are first investigated, and the effects of the computational setup on the NO_x formation are quantified. Then, reaction path analyses are conducted to identify the key contributors to the formation of NO_x pollutants. Finally, the performance of the flamelet model in predicting NO_x pollutants is evaluated.

2. Computational setup

In this work, thermodiffusively unstable premixed hydrogen flames stabilized in 2D and 3D computational domains are simulated with DNS. The computational setups are shown in Figure 1. For the 2D computational domain, it is a square field with a length ($L_x = L_y$) of 100 thermal flame thicknesses of the corresponding 1D unstretched premixed flamelet. This domain size is validated to be sufficiently large to not affect the flame dynamics (Berger *et al.* 2019). The unburned mixture of hydrogen-air with an equivalence ratio ϕ_0

of 0.4, a temperature T_0 of 298 K and a pressure p_0 of 1 atm flows into the domain at $y = 0$ with a velocity u_0 of 0.63 m/s. For the corresponding 1D freely propagating premixed flame, the laminar flame speed u_L is calculated to be 0.21 m/s, the flame thickness l_F is 0.62 mm and the adiabatic flame temperature T_{ad} is 1421 K using the FlameMaster package (Pitsch 1998). The inlet fluid velocity is around 2.9 times the laminar flame speed, so that the flame remains within the domain for a sufficient long time interval. In addition, with the selected inlet velocity, the flame front stays away from the inlet boundary to avoid the inlet influence on the flame dynamics. The computational domain is initialized with the 1D freely propagating premixed flame along the y -direction. As in Berger *et al.* (2019), the flame front is perturbed with a weak harmonic function described by $F(y) = A_0 \sin(2\pi x/\lambda)$. The parameter A_0 is the amplitude of the perturbation, and λ is the wavelength of the perturbation. To trigger the flame instabilities, the initial thermochemical quantities are obtained by mapping the 1D flame solutions along the y -direction of the computational domain, and the parameters of A_0 and λ are set to be the same as those in Berger *et al.* (2019), i.e., $A_0 = 7 \cdot 10^{-4}$ m and $\lambda = 7 \cdot 10^{-3}$ m. A periodic boundary condition is applied in the x -direction, while a constant inlet boundary condition is set at $y = 0$ and an outlet boundary condition is specified at $y = L_y$.

For the 3D computational domain, it is a cuboid field with a length of $100 l_F \times 150 l_F \times 100 l_F$ in the x -, y - and z -directions, respectively, as shown in Figure 1(b). The unburned mixture flows into the computational domain from the x - z plane at $y = 0$, and the burned products flow out of the domain through the x - z plane at $y = 150 l_F$. Different from the 2D case, the inlet velocity is set to be 1.044 m/s, which is around 5 times the laminar flame speed. This inlet velocity is higher than that in 2D, since the flame speed in the 3D domain is larger than that in 2D. As in 2D, the initial thermochemical quantities are obtained by mapping the 1D flame solutions along the y -direction according to $F(y) = A_0 \sin(2\pi x/\lambda) \cdot \sin(2\pi z/\lambda)$, where the parameters of A_0 and λ are set to be the same as those in the 2D case. A periodic boundary condition is set in the x - and z -directions, a constant inlet boundary condition is set at $y = 0$ of the x - z plane and the x - z plane at $y = 150 l_F$ is suppressed with an outlet boundary condition.

For both computational setups, the mesh resolution is set to be sufficiently fine so that there are at least 10 grid points to resolve the corresponding flame thickness. For the 2D case, 1024×1024 grid points are uniformly set in the x - and y -directions, respectively, as in Berger *et al.* (2019). For the 3D case, $1024 \times 1536 \times 1024$ grid points are uniformly set in the x -, y - and z -directions, respectively, resulting in about 1.6 billion grid points. The chemical reaction mechanism developed by Glarborg *et al.* (2018) is adopted, which contains 21 species and 109 elementary reactions. Considering the detailed chemistry, the 3D simulation results in nearly 34 billion degrees of freedom. The simulation ran on 36864 cores and consumed 40 million CPU hours to achieve converged results.

3. Modeling method

3.1. Governing equations and numerical scheme

The governing equations for the momentum, species mass fractions and temperature in the low Mach limit (Tomboulides *et al.* 1997) are solved. The mass diffusivity of each species is calculated using the thermal conductivity, density, specific heat capacity of the gas mixture and the Lewis numbers for each species. The constant non-unity Lewis numbers are calculated from the burned gas region of the corresponding 1D unstretched

premixed flamelet. The molecular diffusion due to the Soret effect is considered using the reduced thermal diffusion model proposed by Schlup & Blanquart (2018).

The DNS is performed with the CIAO code (Desjardins *et al.* 2008) using a time- and space-staggered finite-difference reactive Navier-Stokes solver on Cartesian grids. The momentum equations are discretized with a fourth-order-accurate central difference scheme, while a fifth-order, weighted essentially non-oscillatory scheme (Jiang & Shu 1996) is adopted to discretize the species and temperature governing equations. For the time integration, a second-order-accurate Crank-Nicolson scheme (Crank & Nicolson 1947) is utilized. The Poisson equation is solved with the algebraic multigrid (AMG) solver *hypra* Boomer AMG (Falgout & Yang 2002). The symmetric operator splitting method proposed by Strang (1968) is utilized to efficiently advance the stiff advection-diffusion-reaction equations for species and temperature. A time-implicit backward difference method is employed to integrate the chemical source terms, as implemented in the stiff ODE solver CVODE as part of the SUNDIALS suite (Hindmarsh *et al.* 2005).

3.2. Reaction path analysis

Reaction pathway analyses are conducted to quantify the importance of different NO_x formation pathways in the thermodiffusively unstable premixed hydrogen flame. In the reaction path analysis, the flux is calculated based on the molecular element conservation (Androulakis *et al.* 2004). For instance, the flux of element N between species A and species C in reaction j of $A + B \leftrightarrow C + D$, $\dot{\mathcal{L}}_{AjC}$, is calculated according to

$$\dot{\mathcal{L}}_{AjC} = \frac{n_{N,A} \cdot n_{N,C}}{\mathcal{E}_N} M_N \cdot \dot{\omega}_j, \quad (3.1)$$

where $n_{N,A}$ and $n_{N,C}$ are the number of atom N in species A and species C, respectively. The parameter \mathcal{E}_N is the sum of the number of atom N on either side of the reaction j , M_N the molecular weight of the element N and $\dot{\omega}_j$ the net reaction rate of reaction j . Considering all reactions that convert species A to species C, the net reaction flux of element N between the two species can be calculated as

$$\dot{\mathcal{L}}_{AC} = \sum_{j=1}^{N_r} \dot{\mathcal{L}}_{AjC}, \quad (3.2)$$

where N_r is the number of reactions in the chemical reaction mechanism. To investigate the relative importance of the flux between species A and species C with respect to the other fluxes, the flux ratio ξ_{AC} is introduced, which is calculated by normalizing the individual flux to the magnitude of the sum of the flux between N₂ and the other species,

$$\xi_{AC} = \frac{\dot{\mathcal{L}}_{AC}}{\left| \sum_{k=1}^{N_r} \dot{\mathcal{L}}_{N_2,k} \right|} \times 100\%, \quad (3.3)$$

where $\dot{\mathcal{L}}_{N_2,k}$ is the flux between N₂ and species k .

3.3. A-priori analysis of flamelet model

In this work, the performance of the flamelet model in predicting the NO_x species in the thermodiffusively unstable premixed hydrogen flame is evaluated through an *a-priori* analysis. The flamelet table is generated by solving 1D freely propagating premixed flames at an unburned gas temperature of 298 K and a pressure of 1 atm for various equivalence ratios ranging from 0.32 to 2. The chemical reaction mechanism and the

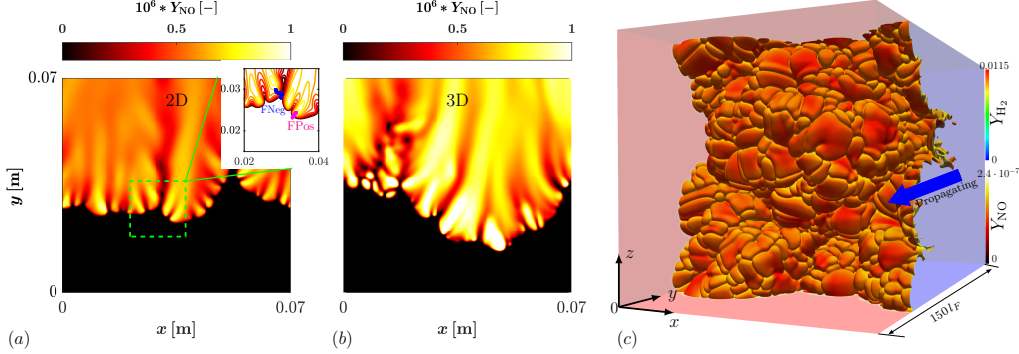


FIGURE 2. Contour plots of NO mass fraction in (a) 2D and (b,c) 3D domains. Two representative flame segments (FNeg in blue and FPos in magenta) extracted along the gradient direction of the progress variable are superimposed in the inset of (a). In (b), the 2D x - y plane ($0 \leq y \leq 100 l_F$) at $z = 50 l_F$ of the 3D domain is shown. In (c), the isosurface of $T_{iso} = 1000$ K colored by the local value of Y_{NO} is shown for illustration of the cellular flame structure.

transport model used in the flamelet table generation are the same as those in the DNS. The thermochemical quantities Ψ in the resulting flamelet table are tabulated as a function of the Bilger mixture fraction Z_{Bilger} (Bilger *et al.* 1990) and normalized progress variable PV , i.e., $\Psi = \mathcal{F}(Z_{Bilger}, PV)$. The variables Z_{Bilger} and PV are defined as

$$Z_{Bilger} = \frac{(Z_H - Z_{H,2})/2M_H - (Z_O - Z_{O,2})/M_O}{(Z_{H,1} - Z_{H,2})/2M_H - (Z_{O,1} - Z_{O,2})/M_O}, \quad PV = \frac{Y_{PV} - Y_{PV,u}}{Y_{PV,b} - Y_{PV,u}}, \quad (3.4)$$

where Z_H and Z_O are the local mixture fraction of elements H and O, respectively. The subscripts 1 and 2 indicate pure fuel and pure air, respectively. In this work, Y_{PV} is defined as $Y_{PV} = Y_{H_2O} - Y_{H_2} - Y_{O_2}$ following previous works (Wen *et al.* 2022a,b). The parameters $Y_{PV,u}$ and $Y_{PV,b}$ in Eq. (3.4) are the corresponding values on the unburned and burned sides, respectively.

In the *a-priori* analysis, Z_{Bilger} and PV are calculated from the DNS. The thermochemical quantities are extracted from the flamelet lookup table (FLT) according to

$$\Psi^{FLT} = \mathcal{F}(Z_{Bilger}^{DNS}, PV^{DNS}). \quad (3.5)$$

The performance of the flamelet model is evaluated by comparing the tabulated values Ψ^{FLT} against the corresponding reference results Ψ^{REF} from the DNS.

4. Results and discussions

4.1. NO_x formation characteristics

The instantaneous distributions of the NO mass fraction Y_{NO} in the 2D and 3D cases are shown in Figure 2. In the 3D domain, the isosurface of $T_{iso} = 1000$ K colored by the local value of Y_{NO} is shown for illustration of the cellular flame structure, with the H_2 mass fraction Y_{H_2} being superimposed as the background color. It can be observed that for both 2D and 3D computational domains, the peak value of Y_{NO} locates at the region with positive curvature κ_c . As in previous works (Berger *et al.* 2019; Wen *et al.* 2022a), the curvature κ_c of the flame front is defined as $\kappa_c = -\nabla \cdot \vec{n} = -\nabla \cdot (\nabla PV / |\nabla PV|)$. In addition, the overall cellular flame structure is significantly different in different computational domains. In the 2D computational domain, a finger-like large

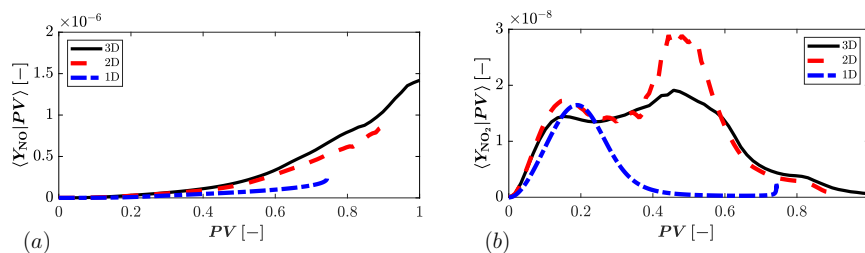


FIGURE 3. Comparing the conditioned NO and NO₂ mass fractions in the progress variable space obtained from 1D, 2D and 3D computational domains for the same operating conditions.

scale flame front can be observed, while in the 3D domain, many differently sized square patches make up the flame front.

To quantitatively investigate the effects of the 2D and 3D domains on the NO_x formation, Figure 3 compares the conditioned NO and NO₂ mass fractions in the normalized *PV* space obtained from the 1D, 2D and 3D computational domains for the same operating conditions. The symbol $\langle \cdot \rangle$ denotes the spatially conditioned values. It can be observed that the peak value of $\langle Y_{NO} \rangle$ in the 3D domain is much higher than that obtained from the 1D and 2D domains. This is considered to be associated with the fact that the 3D flame front corrugations feature higher curvature values, which promotes the accumulation of H₂ due to differential diffusion. For the distribution of $\langle Y_{NO_2} \rangle$ in Figure 3(b), a significantly larger value can be observed in the 2D domain, in the range of $PV = 0.4 \sim 0.8$. The reason for this will be investigated in detail in the next step. Overall, the results show that 3D effects can significantly alter flame propagation and NO_x formation.

4.2. Reaction path analysis

To quantify the relevant reaction pathways that make important contributions to the NO formation, a reaction path analysis was conducted. Figure 4(a) shows the reaction path diagram for the 2D DNS case, which is obtained by integrating over the whole computational domain. The percentages superimposed in the pathway are calculated according to Eq. (3.3). For comparison, the reaction path diagram for the 1D freely propagating premixed flame calculated at the same conditions as in the DNS is shown in Figure 4(b). Only the pathways with percentages larger than 0.1% are shown. The dashed lines in Figure 4(b) indicate the thermal-NO relevant pathways, which are shown even if they are below the 0.1% threshold. The red line indicates the thermal-NO pathway $N + NO \leftrightarrow N_2 + O$, the blue line corresponds to the NNH pathway $NNH \leftrightarrow N_2 + H$ and the violet line is the N₂O pathway $N_2O + M \leftrightarrow N_2 + O + M$. For the operating conditions studied, the NNH and N₂O reaction pathways are much more important than the thermal-NO pathway. The thermal-NO reaction pathway only contributes 0.32% to the N₂ consumption, which is an expected result due to the overall low temperatures ($T_{max} \approx 1600$ K). In addition, the fluxes flowing into NNH (48.9%) are close to those away from NNH (34.8%+6.88%+6.21% = 47.89%), which indicates that the NNH species is in quasi-steady state. For the NO fluxes, the only important pathway for consumption of NO is to form HONO. The corresponding reaction path diagram for the 1D flamelet, shown in Figure 4(b), indicates that the N₂ → NNH pathway becomes less important for the consumption of N₂ compared to the thermodynamically unstable premixed flame studied. The increased importance of the NNH pathway in the thermodynamically unstable

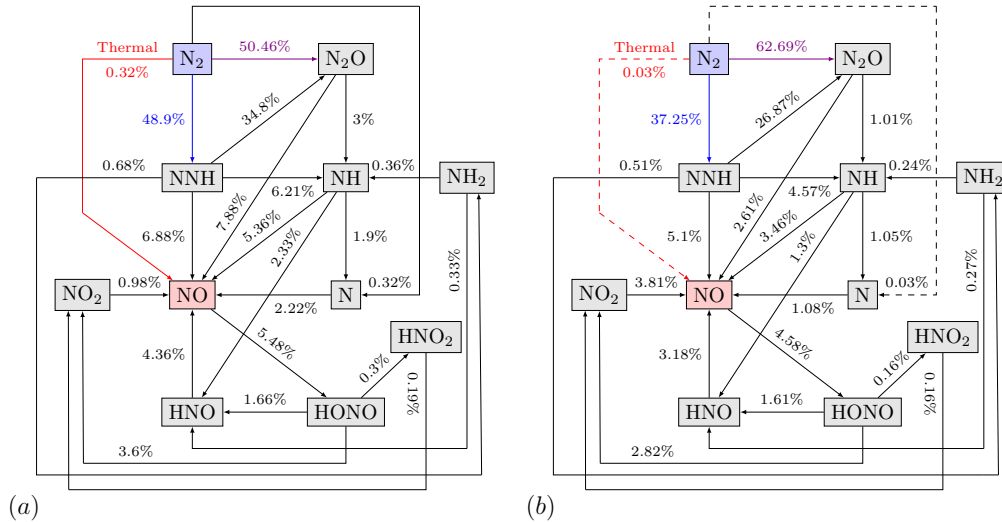


FIGURE 4. Reaction pathway of nitrogen atom obtained from (a) the whole computational domain of the 2D DNS, and (b) the 1D freely propagating premixed flame calculated with the same fresh mixture conditions as in the DNS. The percentages superimposed in the pathway are calculated according to Eq. (3.3). Only the pathways with percentages larger than 0.1% are shown. The thermal-NO-relevant pathways with less weights are indicated in (b) as dashed lines. The red line indicates the thermal-NO pathway $N + NO \leftrightarrow N_2 + O$, the blue line corresponds to the NNH pathway $NNH \leftrightarrow N_2 + H$ and the violet line is the N_2O pathway $N_2O + M \leftrightarrow N_2 + O + M$.

premixed flame is considered to be due to the accumulation of the H radical at positively curved regions, which promotes the NNH formation through $N_2 + H \rightarrow NNH$. Day *et al.* (2011a) reported that the $N_2 \rightarrow NNH$ flux becomes more important as the equivalence ratio of the unburned mixture increases. Thus, the existence of intrinsic instability has locally similar effects to increasing the fuel mixture equivalence ratio. Compared to the 2D DNS, the thermal-NO reaction pathway becomes negligible (0.03%) in the 1D flamelet, which indicates that the thermodiffusive instability promotes the thermal-NO pathway. Such effects are expected to be amplified in fuel-richer or preheated conditions.

Note that the above reaction path analysis and the *a-priori* analysis (see the next section) are currently only based on the 2D data set, while the corresponding analyses for the 3D data set are still ongoing.

4.3. Flamelet modeling of NO_x formation

The performance of the flamelet model in predicting NO_x formation in thermodiffusively unstable premixed hydrogen flames is evaluated through an *a-priori* analysis. The results shown in Figure 2 confirm that the NO_x formation is affected by the flame front corrugations and, hence, curvature. To investigate the effects of curvature on the performance of the flamelet model, two representative flame segments are extracted from the negatively and positively curved regions, given as FNeg and FPos in Figure 2(a).

In Figure 5, the tabulated NO and NO_2 mass fractions and their source terms, referred to as FLT, are compared to the corresponding reference DNS results, referred to as REF. The left column shows the comparison for FNeg representing the negatively curved flame segments, while the right column shows the comparison for FPos representing the positively curved ones. The NO_x species in the positively curved flame segment (FPos) can be accurately predicted by the flamelet model, while discrepancies exist for the

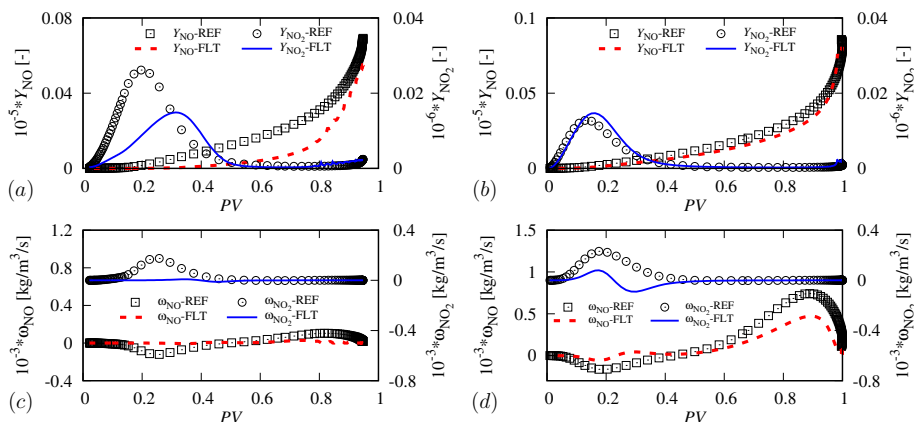


FIGURE 5. Profiles of (a, b) NO_x species mass fractions and (c, d) NO_x reaction source terms, comparing the reference simulation (referred to as REF) and the *a-priori* flamelet predictions (referred to as FLT). The left column shows FNeg, while the right column shows FPos.

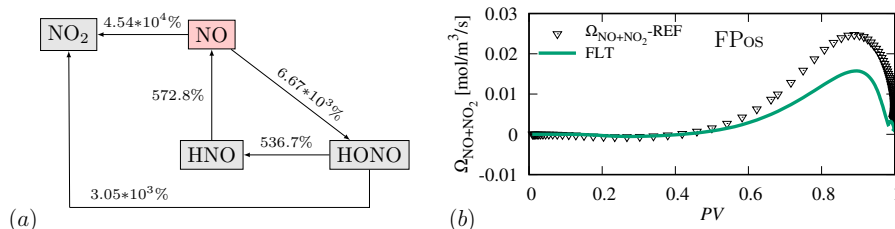


FIGURE 6. (a) Reaction path diagram of nitrogen atom conditioned in the $0.1 < PV < 0.4$ region, as normalized in Figure 4. (b) Profiles of the sum of NO and NO_2 source terms divided by their respective molecular weights, comparing the reference simulation (referred to as REF) and the *a-priori* flamelet predictions (referred to as FLT) for the FPos flame segment.

negatively curved flame segment (FNeg). The budget analysis of the generalized premixed flamelet equations (Wen *et al.* 2022a) shows that the tangential diffusion, which is not considered in the 1D flamelet table, is significant only in the negatively curved flame segments, while it is negligible in the positively curved region. This could be one of the reasons for the inaccurate prediction of the NO_x species in FNeg. For both FNeg and FPos, the reaction source terms cannot be accurately predicted, as shown in Figures 5(c, d). The reason why the prediction accuracy of the NO and N_2O mass fractions is higher than the corresponding source terms could be associated with the fact that the reaction source terms are more sensitive to the local curvature, which is, however, not considered in the flamelet table. From the profiles of NO and NO_2 source terms, it can be observed that the production of NO_2 is significant only in the $0.1 < PV < 0.4$ region, while the production of NO mainly takes place in the region with $PV > 0.6$.

To investigate the reactions in the small progress variable region, a conditioned reaction path analysis is conducted for FPos and the results are shown in Figure 6(a). The flux magnitude of the $\text{NO} \rightarrow \text{NO}_2$ pathway is dominant and is at least one order of magnitude larger than the others. Note that the significant flux ratio is due to the normalization. This indicates that in the small progress variable region, the main reaction is to convert NO to NO_2 . Figure 6(b) shows the comparison of $\dot{\Omega}_{\text{NO}+\text{NO}_2} = (\dot{\omega}_{\text{NO}}/M_{\text{NO}} + \dot{\omega}_{\text{NO}_2}/M_{\text{NO}_2})$ between the flamelet predictions and the reference results for the FPos flame segment.

The value of $\dot{\Omega}_{\text{NO}+\text{NO}_2}$ is close to zero in the $0.1 < PV < 0.4$ range, which is predicted. This indicates that NO_x formation is in a quasi-steady state close to the unburned side. The NO_x species is mainly produced in the range of $PV > 0.6$, which is, however, underpredicted by the flamelet model.

5. Conclusions

NO_x formation in thermodiffusively unstable premixed hydrogen flames is investigated through DNS. To quantify the effects of the computational setup on NO_x formation, both 2D and 3D configurations are considered. The results show that for both 2D and 3D configurations, the peak NO mass fraction occurs at the positively curved regions. In the 3D domain, various sizes of square patches can be observed that do not exist in the 2D domain. The peak value of NO mass fraction in the 3D domain is larger than that in the 1D and 2D domains, while locally high values of NO₂ mass fraction can be observed in the 2D domain. The reaction path analysis shows that the NNH and N₂O pathways are dominant, while the thermal-NO pathway is negligible for the fuel-lean premixed flame studied. The NNH species is in quasi-steady state in the thermodiffusively unstable premixed flame. Compared to the 1D flamelet, the existence of thermodiffusive instability tends to increase the importance of the N₂ → NNH pathway due to differential diffusion of the H radical, which is similar to the effect of an increase of the equivalence ratio. The NO_x species in the positively curved region can be accurately predicted by the flamelet model, while large discrepancies exist in the negatively curved region. For the reaction source terms of the NO_x species, the flamelet model cannot give accurate predictions due to the curvature effects. It is found that the NO in the cooler flame regions is governed by the NO₂ ↔ NO pathway, and that the flamelet model can accurately predict the relevant pathway in the cooler regions but not in the hot regions.

In future work, the influence of the computational setup on the consumption speed and flame surface area will be quantified, and the analyses conducted in this work will be extended to analyze the 3D DNS data set. Furthermore, the flamelet model will be further extended in order to accurately predict the NO_x reaction source terms in the thermodiffusively unstable premixed hydrogen flame.

Acknowledgments

The authors thank Thierry Poinsot, Andrea Aniello and Davide Laera for fruitful discussions during the CTR Summer Program. Computational resources are provided by the Gauss Centre for Supercomputing e.V. on the GCS Supercomputer SuperMUC-NG at Leibniz Supercomputing Centre.

REFERENCES

- ANDROULAKIS, I. P., GREYD, J. M. & BOZZELLI, J. W. 2004 Time-integrated pointers for enabling the analysis of detailed reaction mechanisms. *AIChE J.* **50**, 2956–2970.
- BERGER, L., ATTILI, A. & PITSCH, H. 2022 Intrinsic instabilities in premixed hydrogen flames: parametric variation of pressure, equivalence ratio, and temperature. Part 2 – Non-linear regime and flame speed enhancement. *Combust. Flame* **240**, 111936.
- BERGER, L., KLEINHEINZ, K., ATTILI, A. & PITSCH, H. 2019 Characteristic patterns of thermodiffusively unstable premixed lean hydrogen flames. *Proc. Combust. Inst.* **37**, 1879–1886.

- BILGER, R., STÅRNER, S. & KEE, R. 1990 On reduced mechanisms for methane/air combustion in nonpremixed flames. *Combust. Flame* **80**, 135–149.
- CORREA, S. M. 1993 A review of NO_x formation under gas-turbine combustion conditions. *Combust. Sci. Technol.* **87**, 329–362.
- CRANK, J. & NICOLSON, P. 1947 A practical method for numerical evaluation of solutions of partial differential equations of the heat-conduction type. In *Math. Proc. Camb. Phil. Soc.*, Vol. 43, pp. 50–67. Cambridge University Press.
- DAY, M. S., BELL, J. B., GAO, X. & GLARBORG, P. 2011*a* Numerical simulation of nitrogen oxide formation in lean premixed turbulent $\text{H}_2/\text{O}_2/\text{N}_2$ flames. *Proc. Combust. Inst.* **33**, 1591–1599.
- DAY, M. S., GAO, X. & BELL, J. B. 2011*b* Properties of lean turbulent methane-air flames with significant hydrogen addition. *Proc. Combust. Inst.* **33**, 1601–1608.
- DESJARDINS, O., BLANQUART, G., BALARAC, G. & PITSCH, H. 2008 High order conservative finite difference scheme for variable density low Mach number turbulent flows. *J. Comput. Phys.* **227**, 7125–7159.
- FALGOUT, R. D. & YANG, U. M. 2002 *hypre*: A library of high performance preconditioners. In *Int. Conf. Comput. Sci.*, pp. 632–641.
- GLARBORG, P., MILLER, J. A., RUSCIC, B. & KLIPPENSTEIN, S. J. 2018 Modeling nitrogen chemistry in combustion. *Prog. Energy Combust. Sci.* **67**, 31–68.
- HINDMARSH, A. C., BROWN, P. N., GRANT, K. E., LEE, S. L., SERBAN, R., SHUMAKER, D. E. & WOODWARD, C. S. 2005 SUNDIALS: Suite of nonlinear and differential/algebraic equation solvers. *ACM TOMS* **31**, 363–396.
- JIANG, G.-S. & SHU, C.-W. 1996 Efficient implementation of weighted ENO schemes. *J. Comput. Phys.* **126**, 202–228.
- LAW, C. & SUNG, C. 2000 Structure, aerodynamics, and geometry of premixed flamelets. *Prog. Energy Combust. Sci.* **26**, 459–505.
- MATALON, M. 2007 Intrinsic flame instabilities in premixed and nonpremixed combustion. *Annu. Rev. Fluid Mech.* **39**, 163–191.
- PETERS, N. 1984 Laminar diffusion flamelet models in non-premixed turbulent combustion. *Prog. Energy Combust. Sci.* **10**, 319–339.
- PITSCH, H. 1998 FlameMaster: A C++ computer program for 0D combustion and 1D laminar flame calculations. RWTH Aachen University.
- SCHLUP, J. & BLANQUART, G. 2018 A reduced thermal diffusion model for H and H_2 . *Combust. Flame* **191**, 1–8.
- STRANG, G. 1968 On the construction and comparison of difference schemes. *SIAM J. Numer. Anal.* **5**, 506–517.
- TOMBOULIDES, A., LEE, J. & ORSZAG, S. 1997 Numerical simulation of low Mach number reactive flows. *J. Sci. Comput.* **12**, 139–167.
- WEN, X., ZIRWES, T., SCHOLTISSEK, A., BÖTTLER, H., ZHANG, F., BOCKHORN, H. & HASSE, C. 2022*a* Flame structure analysis and composition space modeling of thermodynamically unstable premixed hydrogen flames—Part I: Atmospheric pressure. *Combust. Flame* **238**, 111815.
- WEN, X., ZIRWES, T., SCHOLTISSEK, A., BÖTTLER, H., ZHANG, F., BOCKHORN, H. & HASSE, C. 2022*b* Flame structure analysis and composition space modeling of thermodynamically unstable premixed hydrogen flames—Part II: Elevated pressure. *Combust. Flame* **238**, 111808.